Optical absorption window in Na_3Bi based three-dimensional Dirac electronic system

Optical absorption window in Na_3Bi based three-dimensional Dirac electronic system

Q. N. Li,[1] W. Xu,[1,2,a)] Y. M. Xiao,[1] L. Ding,[1] B. Van Duppen,[3] and F. M. Peeters[1,3]

[1)] *School of Physics and Astronomy and Yunnan Key Laboratory for Quantum Information, Yunnan University, Kunming 650504, China*

[2)] *Key Laboratory of Materials Physics, Institute of Solid State Physics, Chinese Academy of Sciences, Hefei 230031, China*

[3)] *Department of Physics, University of Antwerp, Groenenborgerlaan 171, B-2020 Antwerpen, Belgium*

(Dated: 18 September 2020)

We present a detailed theoretical study of the optoelectronic properties of a Na_3Bi-based three-dimensional Dirac electronic system (3DDES). The optical conductivity is evaluated using the energy-balance equation derived from a Boltzmann equation, where the electron Hamiltonian is taken from a simplified $\mathbf{k}\cdot\mathbf{p}$ approach. We find that for short-wavelength irradiation, the optical absorption in Na_3Bi is mainly due to inter-band electronic transitions. In contrast to the universal optical conductance observed for graphene, the optical conductivity for Na_3Bi based 3DDES depends on the radiation frequency but not on temperature, carrier density and electronic relaxation time. In the radiation wavelength regime of about $5\ \mu m < \lambda < 200\ \mu m$, an optical absorption window is found. This is similar to what is observed in graphene. The position and width of the absorption window depend on the direction of the light polarization and sensitively on temperature, carrier density, and electronic relaxation time. Particularly, we demonstrate that the inter-band optical absorption channel can be switched on and off by applying the gate voltage. This implies that similar to graphene, Na_3Bi based 3DDES can also be applied in infrared electro-optical modulators. Our theoretical findings are helpful in gaining an in-depth understanding of the basic optoelectronic properties of recently discovered 3DDESs.

I. INTRODUCTION

Since the discovery of graphene[1], extensive theoretical and experimental investigations have been carried on Dirac electronic systems[2]. They exhibit unique and important physical properties that are different from conventional electronic materials such as metals, semiconductors, oxides, etc. In a two-dimensional (2D) Dirac system such as graphene, the electrons are massless and have a gapless and linear-like energy dispersion. These features lead to excellent electronic, transport and optical properties applicable in advanced electronic and optoelectronic devices. Akin to 2D Dirac electronic systems which are normally realized in atomically thin material structures, three-dimensional (3D) Dirac electronic systems (3DDESs) have been recently discovered[3]. These 3DDESs are normally bulk-like with topological electronic structures. At present, the most popularly studied 3DDESs are based on Cd_3As_2[4] and Na_3Bi[5] semi-metals. Such 3DDESs are also gapless and have approximately a linear energy dispersion for the bulk states in conduction and valence bands around the topologically protected Dirac points[3]. In these materials, the crystal inversion symmetry or the time-reversal symmetry is broken so that each Dirac node splits into a pair of opposite-chirality Weyl nodes and a Berry curvature can be achieved in the electronic band structure. As a result, many unique and novel physical phenomena can be observed in 3DDESs, such as chiral electro-[6] and magneto-transport[7], magnetoelectric-like plasmons and photons[8], Fermi-arc surface states[9], chiral-pumping effect[10], nontrivial π Berry phase of Dirac fermions[11], 3D quantum Hall effect[12], etc. These interesting and important research findings demonstrate that the field of 3DDESs is very rich not only in fundamental physics but also in potential applications of 3DDESs in advanced electronic and optoelectronic devices.

Up to now, the study of Na_3Bi based 3DDESs has been mainly focused on their electronic structure, electric and magneto transport and plasmonic properties. Relatively less research has been published on its optoelectronic properties. Experimentally it was demonstrated that 3DDESs can be applied as infrared photodetectors and ultrafast optical switches[13,14]. Very recently, 3DDESs have been applied for terahertz (THz) high harmonic generation[15]. For basic study and device application of 3DDESs in optoelectronics, it is of great importance to examine their fundamental optical properties, which is the prime motivation of the present study.

In 2DDESs such as graphene, interesting and important optoelectronic properties have been observed and investigated. In particular, it has been found that graphene is a wide-band optoelectronic material[16–18] with unique electronic and optical properties. In the short-wavelength regime (visible to near-infrared), the optical conductivity of graphene is caused by inter-band electronic transitions and is universal[19]. The optical absorption channel can be turned on and off by varying the Fermi energy or electron density in graphene as can be realized, e.g., by applying a gate voltage[20,21]. In the long-wavelength regime (terahertz bandwidth), the optical conductivity in graphene is induced by free-carrier optical absorption and increases with radiation frequency[22]. In the intermediate-wavelength regime (mid- to far-infrared), an optical absorption window can be observed[19,22,23], which is a consequence of the fact that different photon energies are required for inter- and intra-band electronic transitions. The width and depth of

[a)] Electronic mail: wenxu_issp@aliyun.com

this window depend strongly on temperature and the carrier density in graphene. These important features have been utilized to realize graphene-based infrared detectors at ambient condition and electro-optical modulators[24,25]. For 3DDESs, because of the different electronic band structure, i.e., the 3D nature of electron motion and the presence of the Berry curvature in the electron energy spectrum, one would expect that the basic features of the electronic transition accompanied by the absorption of photons can differ significantly from 2DDESs.

In this study, we intend to reveal and examine these features and to compare them with those already observed experimentally for graphene. We focus our attention on Na_3Bi-based 3DDESs. At present, high-quality hexagon plate-like Na_3Bi crystals with large (001) plane surfaces can be grown from a molten Na flux[26] and the features of 3D Dirac fermions can be clearly achieved[5,27]. Optical measurements and band structure calculations are reported on Na_3Bi-based three-dimensional Dirac materials[28]. Our goal is to investigate the basic optoelectronic properties of the semi-metal Na_3Bi. Particularly, we look into the effect of the Berry curvature and the crystal orientation of Na_3Bi on optical response. From our theoretical results, we explore the possible application of 3DDESs as novel optoelectronic materials and devices.

Generally, there are three theoretical approaches (Boltzmann equation, quantum Boltzmann equation, and Kubo-Greenwood formalism) to study the optoelectronic properties of the materials and the various theoretical approaches are in agreement with each other[29]. For our theoretical research, because we are considering a three-dimensional system with a low-energy level and a weak radiation field, the energy-balance equation derived from a Boltzmann equation can describe the process of the optical absorption very well. The energy band parameters of Na_3Bi can be calculated by fitting the energy spectrum of the effective Hamiltonian with those obtained from *ab initio* calculations[27].

This paper is organized as follow. The theoretical approaches to calculate the electronic band structure, the electron-photon interaction and the optical conductivity in Na_3Bi semimetal are presented in Section II. In Section III, we present and discuss the numerical results for the optoelectronic properties of Na_3Bi based 3DDES. Our concluding remarks are summarized in Section IV.

II. THEORETICAL APPROACH

A. Simplified electronic band structure

In this study, we take Na_3Bi as an example to study the basic optoelectronic properties of 3DDESs. Na_3Bi is a hexagonal crystal with normally the $P6_3/mmc$ or D^4_{6h} phase[27]. There are two nonequivalent Na sites noted as Na(1) and Na(2). Na(1) and Bi can form simple honeycomb lattice layers stacked along the c-axis. The Na(2) atoms are sandwiched between the above-mentioned lattice layers and connect to the Bi atoms in forming the layers of honeycomb lattices. Na_3Bi has an inverted band structure and its Fermi surface consists of two isolated Fermi points[27]. Both time-reversal and inversion symmetries are present in Na_3Bi so that there is fourfold degeneracy at each Fermi point around which the band dispersion can be linearized. Due to the lattice structure, asymmetric features of the electronic band structure can be expected for Na_3Bi Dirac fermions. The Hamiltonian for relatively low-energy electrons in the semi-metal Na_3Bi can be described within a $\mathbf{k}\cdot\mathbf{p}$ approximation[27], which reads

$$H(\mathbf{K}) = \varepsilon(\mathbf{K})\times I + \begin{pmatrix} M_{\mathbf{K}} & Ak_+ & 0 & B^*_{\mathbf{K}} \\ Ak_- & -M_{\mathbf{K}} & B^*_{\mathbf{K}} & 0 \\ 0 & B_{\mathbf{K}} & M_{\mathbf{K}} & -Ak_- \\ B_{\mathbf{K}} & 0 & -Ak_+ & -M_{\mathbf{K}} \end{pmatrix}, \quad (1)$$

where $\mathbf{K} = (\mathbf{k}, k_z) = (k_x, k_y, k_z)$ is the electron wave-vector or momentum operator, and I is a 4×4 unitary matrix. The z-direction is taken along the stacking direction of the honeycomb lattice layers formed by Na(1) and Bi, $k_\pm = k_x \pm ik_y$, $\varepsilon(\mathbf{K}) = C_0 + C_1k_z^2 + C_2k^2$, $M_{\mathbf{K}} = M_0 - M_1k_z^2 - M_2k^2$, and C_0, C_1, C_2, M_0, M_1, M_2 and A are band parameters[27]. In this Hamiltonian, $B_{\mathbf{K}} = B_3k_zk_+^2 \sim K^3$ gives a high-order contribution to the electron motion, which is significant only at relatively large electron momentum. The corresponding Schrödinger equation can be solved analytically and the eigenvalues are obtained as $E_\pm(\mathbf{K}) = \varepsilon(\mathbf{K}) \pm \sqrt{M_{\mathbf{K}}^2 + A^2k^2 + |B_{\mathbf{K}}|^2}$, where the upper (lower) case refers to conduction (valence) band. In this electronic system, two Dirac points exist at $k = 0$ and $k_z = \pm k_c = \pm\sqrt{M_0/M_1}$. The eigenvalue of this Hamiltonian can be in a good agreement with the experimental work[5] at about $0.8\ eV$.

Now, we consider the electrons interacting with a radiation field via the direct optical transition mechanism. Under the action of a weak radiation field with relatively low photon energies, the electronic response to the radiation field is dominated by low-energy and small-momentum electrons. Similar to a conventional semiconductor, the electronic transition accompanied by the absorption of photons in a 3DDES is achieved mainly from occupied electronic states to empty states around the Fermi energy without change of electron momentum. In this case, we can limit ourselves to low-energy and small-momentum electrons and neglect the high-order terms $B_{\mathbf{K}} \sim K^3 \ll 1$ in Eq. (1). Thus, the block-diagonal form allows us to decouple the 4×4 matrix given by Eq. (1) into a simplified 2×2 matrix, which reads

$$H(\mathbf{K}) = \begin{pmatrix} \varepsilon(\mathbf{K}) + M_{\mathbf{K}} & Ak_+ \\ Ak_- & \varepsilon(\mathbf{K}) - M_{\mathbf{K}} \end{pmatrix}. \quad (2)$$

By solving the corresponding Schrödinger equation, an analytical expression for the eigenvalue and eigenfunction are obtained, respectively, as

$$E_\lambda(\mathbf{K}) = \varepsilon(\mathbf{K}) + \lambda\sqrt{M_{\mathbf{K}}^2 + A^2k^2}, \quad (3)$$

and

$$\psi_{\lambda\mathbf{K}}(\mathbf{R}) = |\mathbf{K},\lambda\rangle = a_{\mathbf{K}} \begin{pmatrix} 1 \\ b_{\mathbf{K}} \end{pmatrix} e^{i\mathbf{K}\cdot\mathbf{R}}, \quad (4)$$

with $\mathbf{R} = (x,y,z)$, $a_{\mathbf{K}} = Ak(\xi_{\lambda\mathbf{K}}^2 + A^2k^2)^{-1/2}$, $b_{\mathbf{K}} = \lambda\xi_{\lambda\mathbf{K}}/Ak_-$, $k = \sqrt{k_x^2 + k_y^2}$, $\xi_{\lambda\mathbf{K}} = \sqrt{M_{\mathbf{K}} + A^2k^2} - \lambda M_{\mathbf{K}}$, and

$\lambda = +1$ refers to conduction band and $\lambda = -1$ to valance band. In this simplified $\mathbf{k}\cdot\mathbf{p}$ Hamiltonian, we can see that the two Dirac points are still present at $k = 0$ and $k_z = \pm k_c = \pm\sqrt{M_0/M_1}$. The energy splitting induced by the presence of the $B_{\mathbf{K}} = B_3 k_z k_+^2$ terms in Eq. (1) is rather weak for the case of relatively small k. Even if we take $B_3 = 50\ eV\AA^3$ and $100\ eV\AA^3$, which are rather large values for Na_3Bi, the effect of band splitting is still very small[30]. This is similar to the case of Cd_3As_2-based 3D Dirac systems in which the effect of band splitting is weak[31]. As a result, the neglect of the $B_{\mathbf{K}}$ term in Eq. (1) does not significantly affect the electronic band structure in the momentum and energy domains in which we are interested. Therefore, from now on in this study we take the simplified electron Hamiltonian given by Eq. (2). Very recently, we have applied this electronic band structure for the investigation of the electronic transport properties of Na_3Bi based 3DDES[30] and good agreement between theoretical and experimental[32,33] results was achieved.

B. Carrier-photon interaction

In the present study, we use our previous theoretical approach that we developed for investigating of the optoelectronic properties for graphene[34] to calculate the optical conductivity for a 3DDES. Here we consider electrons in a 3DDES interacting with a linearly polarized radiation field as a continuous wave (CW). Because of the asymmetric electronic energy spectrum, as given by Eq. (3), the polarization direction along the xy-plane (here taken along the x-direction) and along the z-direction have to be considered separately. Including the effect of the radiation field within the usual Coulomb gauge, the carrier-photon interaction Hamiltonian can be obtained by taking $\mathbf{K} \to \mathbf{K} - e\mathbf{A}(t)$ in Eq. (2) with $\mathbf{A}(t)$ being the vector potential of the radiation field. Next, $H(\mathbf{K} - e\mathbf{A}(t))$ is expanded as $H(\mathbf{K} - e\mathbf{A}(t)) \simeq H(\mathbf{K}) + H'(t)$. For the case of weak radiation intensity, we can neglect the higher order effect with $A^2(t)$ terms. For the cases where light polarization is along the x- and the z-direction of Na_3Bi, the carrier-photon interaction Hamiltonian can be written respectively as

$$H'_x(t) = \frac{2eA(t)}{\hbar}\begin{pmatrix} (M_2 - C_2)k_x & -A/2 \\ -A/2 & -(M_2 + C_2)k_x \end{pmatrix}, \tag{5}$$

and

$$H'_z(t) = \frac{2eA(t)k_z}{\hbar}\begin{pmatrix} (M_1 - C_1) & 0 \\ 0 & -(M_1 + C_1) \end{pmatrix}, \tag{6}$$

where $A(t) = (F_0/\omega)\sin(\omega t)$ for a CW radiation field, F_0 is the electric field strength of the light field, and ω is its frequency. Because we limit ourselves to the case of weak radiation field, we neglect the contribution from F_0^2 terms. As we can see from Eqs. (5) and (6), when the radiation is polarized linearly along different directions the carrier-photon interaction Hamiltonian takes different functional forms.

The first-order steady-state electronic transition rate induced by carrier-photon interactions via photon absorption scattering in Eq. (5) and Eq. (6) can be obtained using the Fermi's golden rule, which reads

$$W^j_{\lambda\lambda'}(\mathbf{K},\mathbf{K}') = \frac{2\pi}{\hbar}\left(\frac{eF_0}{\omega\hbar}\right)^2 |U^j_{\lambda\lambda'}(\mathbf{K})|^2 \delta_{\mathbf{K}',\mathbf{K}} \times \delta[E_{\lambda'}(\mathbf{K}') - E_{\lambda}(\mathbf{K}) - \hbar\omega] \tag{7}$$

with $j = x$ or z. This is the probability for scattering of a carrier from a state $|\mathbf{K},\lambda\rangle$ to a state $|\mathbf{K}',\lambda'\rangle$ induced by the interaction with the linearly polarized radiation field, accompanied by the absorption of a photon with energy $\hbar\omega$. Here,

$$|U^j_{\lambda\lambda'}(\mathbf{K})|^2 = \frac{|G^j_{\lambda\lambda'}(\mathbf{K})|^2}{[\xi^2_{\lambda\mathbf{K}} + A^2k^2][\xi^2_{\lambda'\mathbf{K}} + A^2k^2]}, \tag{8}$$

with

$$G^x_{\lambda\lambda'}(\mathbf{K}) = A^2(\lambda k_+ \xi_{\lambda\mathbf{K}} + \lambda' k_- \xi_{\lambda'\mathbf{K}})/2 - k_x[A^2k^2(M_2 - C_2) - \lambda\lambda'(M_2 + C_2)\xi_{\lambda\mathbf{K}}\xi_{\lambda'\mathbf{K}}],$$

and

$$G^z_{\lambda\lambda'}(\mathbf{K}) = k_z[A^2k^2(M_1 - C_1) - (M_1 + C_1)\lambda\lambda'\xi_{\lambda\mathbf{K}}\xi_{\lambda'\mathbf{K}}].$$

C. Optical conductivity

In this work, we employ the Boltzmann equation as the governing transport equation to study the response of carriers in Na_3Bi to an applied light field. The semi-classical Boltzmann equation can be written as

$$\frac{\partial f_\lambda(\mathbf{K})}{\partial t} = g_s \sum_{\lambda',\mathbf{K}'} [F^j_{\lambda\lambda'}(\mathbf{K},\mathbf{K}') - F^j_{\lambda'\lambda}(\mathbf{K}',\mathbf{K})] \tag{9}$$

where $g_s = 2$ counts for for spin degeneracy, $f_\lambda(\mathbf{K})$ is the momentum-distribution function for a carrier at state $|\mathbf{K},\lambda\rangle$ and $F^j_{\lambda\lambda'}(\mathbf{K},\mathbf{K}') = f_\lambda(\mathbf{K})[1 - f_{\lambda'}(\mathbf{K}')]W^j_{\lambda\lambda'}(\mathbf{K},\mathbf{K}')$. Because the radiation field has already been included within the electronic transition rate, the force term induced by the light field does not appear in the drift term on the left-hand side of the Boltzmann equation. Eq. (9) with the electronic transition rate $W^j_{\lambda\lambda'}(\mathbf{K},\mathbf{K}')$ given by Eq. (7) cannot be solved analytically. In this study we employ the usual balance-equation approach[35,36] to approximately solve the problem. By multiplying $g_s\sum_{\lambda,\mathbf{K}} E_\lambda(\mathbf{K})$ to both sides of the Boltzmann equation, Eq. (9), we obtain the energy-balance equation. From the energy-balance equation, we get the energy transfer rate for a carrier in 3DDES: $P^j(\omega) = g_s\sum_{\lambda,\mathbf{K}} E_\lambda(\mathbf{K})\partial f_\lambda(\mathbf{K})/\partial t = \sum_{\lambda\lambda'} P^j_{\lambda\lambda}(\omega)$ with

$$P^j_{\lambda\lambda'}(\omega) = 4\hbar\omega \sum_{\mathbf{K},\mathbf{K}'} F^j_{\lambda\lambda'}(\mathbf{K},\mathbf{K}'). \tag{10}$$

Knowing the electronic energy transfer rate, we can calculate the optical conductivity via[37]: $\sigma_{jj}(\omega) = P(\omega)/(2F_0^2)$. Once the optical conductivity is obtained, we can calculate other optical coefficients such as the absorption and the transmission

coefficients by using basic laws of electrodynamics. The optical conductivity obtained from the energy-balance equation is given by

$$\sigma_{jj}(\omega)=\sum_{\lambda,\lambda'}\sigma_{jj}^{\lambda\lambda'}(\omega)=\frac{2\hbar\omega}{F_0^2}\sum_{\lambda,\lambda'}\sum_{\mathbf{K},\mathbf{K}'}F_{\lambda\lambda'}^{j}(\mathbf{K},\mathbf{K}'). \quad (11)$$

Because $F_{\lambda\lambda'}^{j}(\mathbf{K},\mathbf{K}')\sim F_0^2$ (see Eq. (7)), $\sigma_{jj}(\omega)$ is independent of the radiation intensity F_0 in case F_0 is sufficiently weak.

One of the major advantages of the balance-equation approach is that we can circumvent the difficulties of solving the Boltzmann equation directly by using a specific form of the distribution function. In this study, we assume that the momentum distribution function for carriers in Na_3Bi can be described by a statistical energy distribution such as the Fermi-Dirac function, namely we take $f_\lambda(\mathbf{K})\simeq f_\lambda[E_\lambda(\mathbf{K})]$ with $f_+(x)=[1+e^{(x-E_F^e)/k_BT}]^{-1}$ or $f_-(x)=[1+e^{(x-E_F^h)/k_BT}]^{-1}$ being respectively the Fermi-Dirac function for electrons or holes, where E_F^e and E_F^h are chemical potentials (or Fermi energies at $T\to 0$) for electrons and holes, respectively. It should be noted that similar to a semiconductor, for a n-type Na_3Bi subjected to a radiation field, photon-induced carriers are possible. As a result, the chemical potentials for electrons and holes can be different.

After considering the effect of the broadening of the scattering states due to energy relaxation, i.e., by taking $\delta(E)\to(E_\tau/\pi)(E^2+E_\tau^2)^{-1}$ (where $E_\tau=\hbar/\tau$) in Eq. (7) with τ being the energy relaxation time, we can calculate the optical conductivity induced by different transition channels. For the situation where the radiation field is polarized along the x-direction, the optical conductivity induced by intra-band transitions is obtained as

$$\sigma_{xx}^{\lambda\lambda}(\omega)=\frac{\sigma_0}{A_\omega^2}\frac{\omega\tau}{1+(\omega\tau)^2}\int_0^\infty dk_z\int_0^\infty dkk^3\mathscr{G}_{\lambda\lambda}^{x}(\mathbf{K}) \times f_\lambda(E_\lambda(\mathbf{K}))[1-f_\lambda(E_\lambda(\mathbf{K}))], \quad (12)$$

where $\lambda=\lambda'=\pm1$ refer to conduction and valance band, $\sigma_0=e^2/\hbar$, $A_\omega=\pi\hbar\omega$, and

$$\mathscr{G}_{\lambda\lambda}^{x}(\mathbf{K})=\Big[\frac{A^2[k^2(M_2-C_2)-\lambda\xi_{\lambda\mathbf{K}}]-(M_2+C_2)\xi_{\lambda\mathbf{K}}^2}{\xi_{\lambda\mathbf{K}}^2+A^2k^2}\Big]^2.$$

For inter-band transitions, we have $\sigma_{xx}^{+-}(\omega)\to 0$ because of the Conservation of energy required the electrons transition can only achieve through the lower occupied states to the higher empty states due to the absorption of a photon and

$$\sigma_{xx}^{-+}(\omega)=\frac{\sigma_0A^2\omega\tau}{A_\omega^2}\int_0^\infty dk_z\int_0^\infty dkk\mathscr{G}_{-+}^{x}(\mathbf{K}) \times\frac{f_-(E_-(\mathbf{K}))[1-f_+(E_+(\mathbf{K}))]}{1+(\omega-2\sqrt{M_\mathbf{K}^2+A^2k^2}/\hbar)^2\tau^2}, \quad (13)$$

with

$$\mathscr{G}_{-+}^{x}(\mathbf{K})=1+\frac{(2M_2k^2+M_\mathbf{K})^2}{M_\mathbf{K}^2+A^2k^2}.$$

For the situation of light polarization along the z-direction, the optical conductivity induced by the intra-band transitions is obtained as

$$\sigma_{zz}^{\lambda\lambda}(\omega)=\frac{2\sigma_0}{A_\omega^2}\frac{\omega\tau}{1+(\omega\tau)^2}\int_0^\infty\int_0^\infty dkdk_zkk_z^2 \times\mathscr{G}_{\lambda\lambda}^{z}(\mathbf{K})f_\lambda(E_\lambda(\mathbf{K}))[1-f_\lambda(E_\lambda(\mathbf{K}))], \quad (14)$$

with

$$\mathscr{G}_{\lambda\lambda}^{z}(\mathbf{K})=\Big[\frac{A^2k^2(M_1-C_1)-(M_1+C_1)\xi_{\lambda\mathbf{K}}^2}{\xi_{\lambda\mathbf{K}}^2+A^2k^2}\Big]^2.$$

For inter-band transitions, we have $\sigma_{zz}^{+-}(\omega)\to 0$ and

$$\sigma_{zz}^{-+}(\omega)=\frac{2\sigma_0}{A_\omega^2}A^2M_1^2\omega\tau\int_0^\infty\int_0^\infty\frac{dkdk_zk^3k_z^2}{M_\mathbf{K}^2+A^2k^2} \times\frac{f_-(E_-(\mathbf{K}))[1-f_+(E_+(\mathbf{K}))]}{1+(\omega-2\sqrt{M_\mathbf{K}^2+A^2k^2}/\hbar)^2\tau^2}. \quad (15)$$

Using these equations, we can evaluate the contributions from different transition channels to the optical conductivity or the optical absorption.

III. RESULTS AND DISCUSSION

For numerical calculations, we take the band parameters for Na_3Bi as[27]: $C_0=-0.06382$ eV, $C_1=8.7536$ eVÅ^2, $C_2=-8.4008$ eVÅ^2, $M_0=-0.08686$ eV, $M_1=-10.6424$ eVÅ^2, $M_2=-10.3610$ eVÅ^2, and $A=2.4598$ eVÅ. These parameters were determined by fitting the energy spectrum of the effective Hamiltonian given by Eq. (1) with those obtained from *ab initio* calculations[27]. Furthermore, it has been shown experimentally that in a Na_3Bi 3DDES, the electronic relaxation time is different for samples with different carrier densities[33]. Thus, we take the following $\tau=1.0$ ps, 1.49 ps, 1.94 ps, 2.55 ps and 6.71 ps obtained experimentally[33] in our calculations.

By definition, the condition of carrier number conservation is given by: $N_\lambda=g_s\sum_\mathbf{K}f_\lambda[E_\lambda(\mathbf{K})]$ with N_λ being the electron or hole density. Using this condition, we can determine the corresponding chemical potential E_F for electrons and holes at finite-temperature, which reads

$$N_e=\frac{1}{\pi^2}\int_0^\infty dk_z\int_0^\infty dkkf_+[E_+(\mathbf{K})], \quad (16)$$

for conduction band and

$$N_h=\frac{1}{\pi^2}\int_0^\infty dk_z\int_0^\infty dkk[1-f_-[E_-(\mathbf{K})]], \quad (17)$$

for valance band. Thus, the chemical potential E_F^λ for electrons and holes can be obtained numerically from respectively Eqs. (16) and (17) for given carrier densities N_e and N_h at finite-temperature T. It should be noted that for n-type Na_3Bi, if N_0 is the electron density in the absence of the radiation field (or dark density), the electron density in the presence of

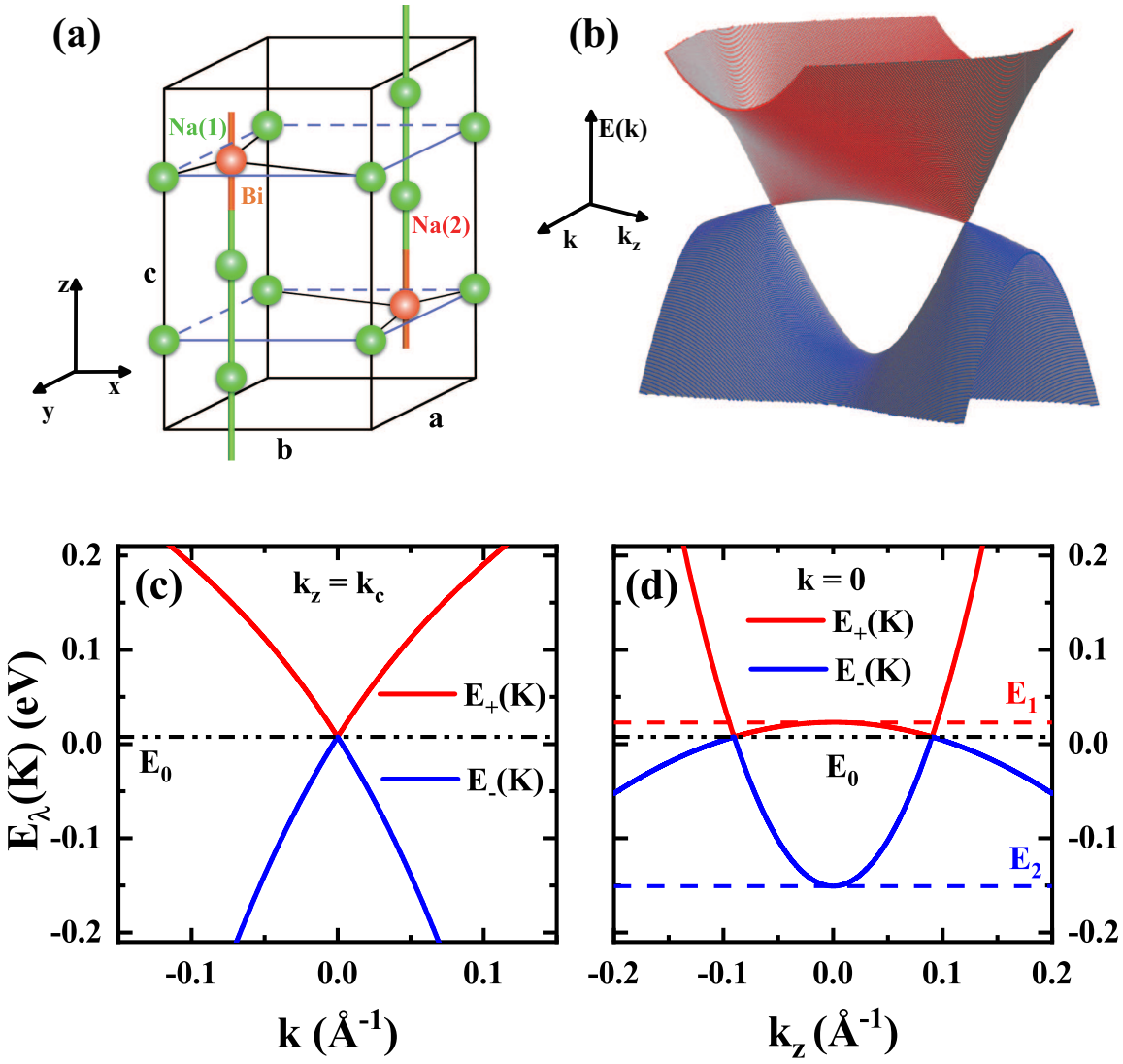

FIG. 1. (a) The Na_3Bi crystal structure. Na(1) and Bi form simple honeycomb lattice layers stacked along the c-axis and Na(2) atoms are sandwiched between the above-mentioned lattice layers and connect to the Bi atoms in forming the layers of honeycomb lattices. (b) The conduction (red) and valance (blue) band energies in a Na_3Bi-based 3DDES as a function of k and k_z, as given by Eq. (3). (c) The electron energy as a function of k at $k_z = k_c$. The band crossing point is at $E_0 \simeq 7.6$ meV for $k = 0$ and $k_z = \pm k_c$ (dashed-dotted line). (d) The electron energy as a function of k_z at $k = 0$. The top of the Berry curvature in the conduction band is $E_1 \simeq 23$ meV and the bottom of the Berry curvature in the valance band is $E_2 \simeq -151$ meV, which are both located at $k = 0$ and $k_z = 0$.

the radiation is $N_e = N_0 + \Delta N_e$, where ΔN_e is the density of photo-excited electrons. Under the condition of charge number conservation, $\Delta N_e = N_h$ is the hole density in the presence of light irradiation.

The features of the conduction band structure of Na_3Bi 3DDES have been discussed previously[30] and will therefore not be repeated. Because inter-band electronic transitions are involved in the present study, here we present and discuss the conduction and valence band structure for semi-metal Na_3Bi. In Fig. 1, we show the crystal structure and energy dispersion relation of a Na_3Bi-based 3DDES, given by Eq. (3) for conduction and valance bands. Fig. 1(a) shows the crystal structure of Na_3Bi as we described in Section II A. The crystal lattice constant $a = b \approx 5.448$ Å and $c \approx 9.665$ Å[27]. In Fig. 1(b), the 3D plot is shown for $E_\lambda(\mathbf{K})$ as function of k and k_z. We see that the electron energy has a different dependence on k and k_z for both conduction and valance bands, showing the asymmetric nature of the electron energy spectrum in the xy-plane and along the z-direction in Na_3Bi 3DDES. In order to see more clearly the Dirac points and the Berry curvature in the energy bands, we show the electron energy as a function of k at a fixed $k_z = k_c$ in Fig. 1(b) and as a function of k_z at $k = 0$ in Fig. 1(c). We note that in the theoretical model, the bottom of the conduction band or the top of the valance band is at

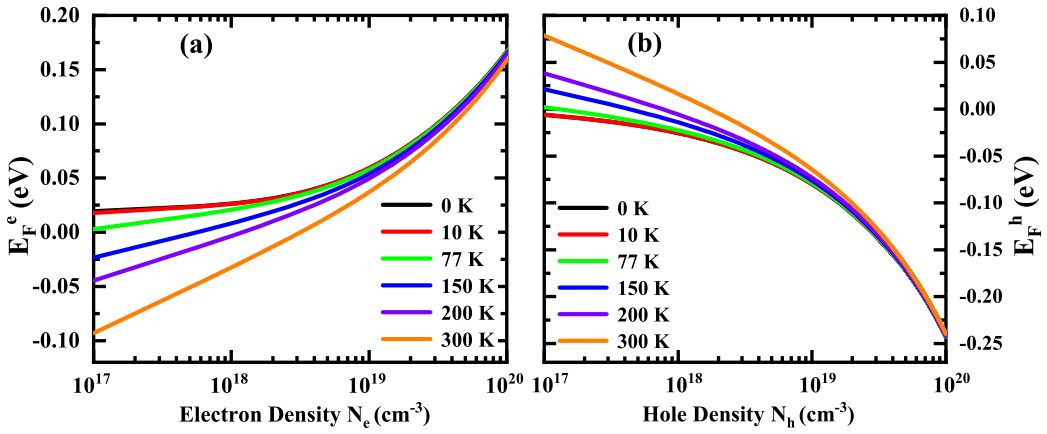

FIG. 2. The chemical potential for electrons E_F^e (a) and for holes (b) in a Na_3Bi based 3DDES as a function of electron density N_e and hole density N_h at different temperatures as indicated. The results for $T = 0$ and $T = 10$ K almost coincide.

$E_0 = 7.6$ meV, which is reached by taking $k = 0$ and $k_z = \pm k_c$ (see Fig. 1(b)). Thus, the energy reference in this study is from $E_0 = 7.6$ meV. From Fig. 1, we notice the following special features: i) two Dirac points can be found at the bottom of the conduction band and the top of the valance band when $k_z = \pm k_c$ and $k = 0$. ii) Around the Dirac points, the electron energies for conduction and valance bands are asymmetric and depend nonlinearly on k and k_z. These features are in sharp contrast to those in graphene. iii) The electronic energy spectrum show arch-bridge-like Berry curvatures in both conduction and valance bands. The effect of the Berry curvature is much stronger in the valance band. The top of the Berry curvature is at $E_1 \simeq 23$ meV in the conduction band and the bottom of the Berry curvature is at $E_2 \simeq -151$ meV in the valance band, which are both reached at $k = k_z = 0$ (see Fig. 1(c)). These features for a 3DDES differ significantly from those for graphene and from conventional 3D electron gas systems.

In Fig. 2, we show the chemical potential E_F^λ as a function of carrier density at different temperatures, where N_e and N_h are respectively the electron and hole density. If there is no conducting carriers in the system, E_F^e and E_F^h reach the Dirac points at about $E_0 = 7.6$ meV at $T \to 0$. Similar to a conventional semiconductor, the Fermi energy for electrons (holes) in a 3DDES increases (decreases) with increasing carrier density but decreases (increases) with increasing temperature. The results shown in Fig. 1 and Fig. 2 suggest that when E_F^e is smaller than $E_0 + E_1 = 30.6$ meV, the electrons are mainly located in the conduction band of the energy range with Berry curvature, which corresponds to an electron density $N_e \sim 4 \times 10^{18}$ cm^{-3}[30]. For n-type Na_3Bi, because of the low hole density generated mainly via optical excitation and of the strong Berry curvature effect, the holes are always located in the valance band energy regime with Berry curvature. Experimentally, the electron density in a n-type Na_3Bi sample can be altered through post-annealing[32,33]. Thus, one can tune the Fermi level inside and outside the Berry curvature regime in order to see anomalous features in, e.g., the conductivity[32,33].

To gain an in-depth understanding of the mechanism for optical response of carriers in a 3DDES, in Fig. 3 we present

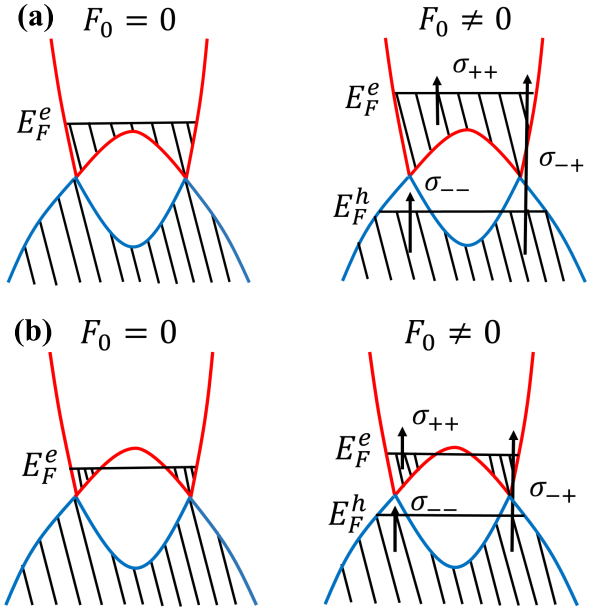

FIG. 3. Schematic diagram of the electronic transitions accompanied by the absorption of a photon in a n-type 3DDES. Here, $F_0 = 0$ and $F_0 \neq 0$ refer respectively to the cases in the absence and presence of the radiation field. E_F^e and E_F^h are respectively the Fermi energy for electrons and holes, and the up-arrows stand for different transition channels with corresponding optical conductivities $\sigma_{\lambda\lambda'}$ induced by intra- and inter-band transition events. Two situations for Fermi energy E_F^e outside [in (a)] and inside [in (b)] the Berry curvature regime are indicated. E_F^h is always inside the Berry curvature regime in the valance band.

schematic diagrams of the electronic transition channels in the absence and presence of a radiation field. In the absence of the radiation field (i.e., $F_0 = 0$), the valance band is fully occupied in a n-type 3DDES and the Fermi energy for electrons crosses the conduction band. In the presence of the radiation field (i.e., $F_0 \neq 0$), electrons in the valance band are excited optically from the valance band to the conduction band. Thus, photon-generated electrons are added to the conduction band and the holes are generated in the valance band along with the creation of the Fermi energy for holes in the valance band. Like in other electronic systems, the optical response of carriers in a 3DDES can be achieved through electronic transitions from the lower occupied states to the higher empty states due to the absorption of a photon. We see from Fig. 3 that the main difference between the different cases where the Fermi energy E_F^e is outside [in (a)] or inside [in (b)] the Berry curvature regime in the conduction band is the density-of-states for initial and final states of the electronic transitions. In the presence of a light field the intra-band electronic transition via optical absorption can be achieved not only in the conduction band via the channel σ_{++} but also in the valence band via the channel σ_{--}. The intra-band transitions are a consequence of direct optical absorption in the 3DDES. Because Na_3Bi is a gapless 3DDES, the electrons in the valence band can be more easily excited optically into the conduction band in contrast to a conventional semiconductor. Thus, there is a strong inter-band transition channel σ_{-+} (in Fig. 3) in Na_3Bi-based 3DDES. These features are similar to those in the 2D Dirac system such as graphene[34]. Since optical absorption is achieved by electronic transitions from occupied states to empty states, together with the presence of the Moss-Burstein effect[38] or the Pauli blockade effect[39], intra-band transitions require less photon energy $\hbar\omega$, whereas a relatively larger photon energy is needed for inter-band transitions. Hence, the intra-band optical absorption in both conduction band σ_{++} and valence band σ_{--} will decrease with increasing photon energy in the long-wavelength regime (or the lower photon energy regime). With a growing photon energy, the intra-band optical absorption will go down to close to 0, meanwhile inter-band optical absorption σ_{-+} will increase rapidly and it becomes the main contribution for the optical conductivity in the larger photon energy regime (in the short-wavelength regime). Consequently, an optical absorption window can be induced through different energy requirements for inter- and intra-band optical absorption between the the long-wavelength regime and the the short-wavelength regime.

In Fig. 4, we show the contributions from different electronic transition channels to the optical conductivity induced by light irradiation with different polarization directions in a Na_3Bi based 3DDES, where $\sigma_{xx}(\omega)$ and $\sigma_{zz}(\omega)$ are shown respectively in the upper and lower panels at fixed temperature $T = 150$ K, electronic relaxation time $\tau = 6.71$ ps, electron density $N_e = 2.0 \times 10^{19}$ cm^{-3}, and hole density $N_h = 2.0 \times 10^{18}$ cm^{-3}. From Fig. 4, we notice: i) the inter-band transitions contribute to the optical conductivity in the short-wavelength regime and the intra-band transitions give rise to the long-wavelength optical conductivity in both $\sigma_{xx}(\omega)$ and $\sigma_{zz}(\omega)$. ii) The short-wavelength optical conductivity in a 3D-

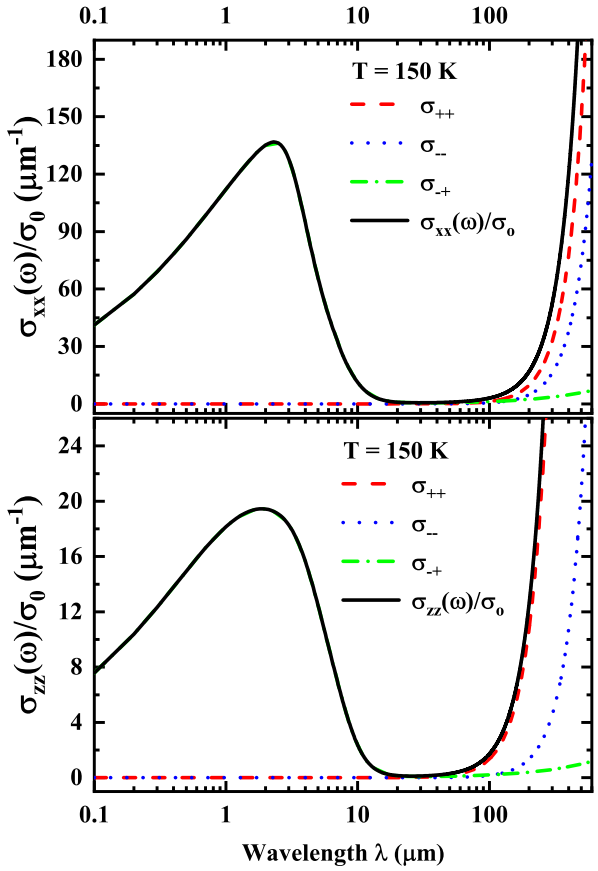

FIG. 4. Contributions from different electronic transition channels to optical conductivity for light radiation polarized linearly along the x-direction $\sigma_{xx}(\omega)$ (upper panel) and along the z-direction $\sigma_{zz}(\omega)$ (lower panel) at the fixed temperature $T = 150$ K, electronic relaxation time $\tau = 6.71$ ps, electron density $N_e = 2.0 \times 10^{19}$ cm^{-3}, and hole density $N_h = 2.0 \times 10^{18}$ cm^{-3}. Here $\sigma_0 = e^2/\hbar$.

DES increases with radiation wavelength when $\lambda < 2\ \mu m$. An optical absorption peak can be observed. This phenomenon differs from graphene in which the optical conductivity is universal[19,20], namely $\sigma(\omega) = e^2/(4\hbar)$ and does not depend on the radiation frequency, temperature and sample parameters such as electron density and scattering strength. iii) In the short-wavelength regime, $\sigma_{xx}(\omega)$ is about 5 times larger than $\sigma_{zz}(\omega)$. This suggests that stronger optical absorption can be achieved when the radiation field is polarized linearly along the 2D-plane of a 3DDES. The optical absorption peak for $\sigma_{xx}(\omega)$ is sharper than that for $\sigma_{zz}(\omega)$. From the electron energy spectrum shown in Fig. 1, we see that $E_\lambda(\mathbf{K})$ for a Na_3Bi based 3DDES depends differently on k and k_z. Because the Berry curvature appears at $k_z = \pm k_c$, the density-of-states (DoS) for electrons along the z-direction is smaller than in the xy plane, so that σ_{xx} is larger than σ_{zz}. iv) More interestingly, both $\sigma_{xx}(\omega)$ and $\sigma_{zz}(\omega)$ show an optical absorption window in the intermediate wavelength regime (about $5\ \mu m < \lambda < 400\ \mu m$ for σ_{xx} and $5\ \mu m < \lambda < 200\ \mu m$ for σ_{zz}), because the optical absorption coefficient is proportional to optical conductivity. This effect is induced by the blocking of the optical ab-

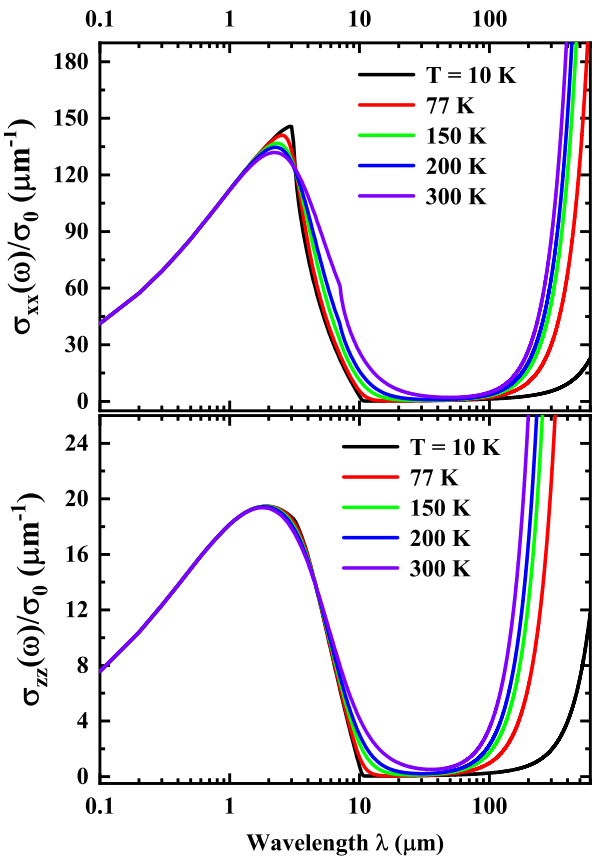

FIG. 5. Optical conductivities $\sigma_{xx}(\omega)$ (upper panel) and σ_{zz} (lower panel) as a function of radiation wavelength at the fixed electronic relaxation time $\tau = 6.71$ ps and carrier densities $N_e = 2.0\times10^{19}$ cm^{-3} and $N_h = 2.0\times10^{18}$ cm^{-3} for different temperatures $T = 10$ K (black curve), 77 K (red curve), 150 K (green curve), 200 K (blue curve), and 300 K (purple curve).

sorption channels due to inter- and intra-band electronic transitions as shown in Fig. 3. Thus, similar to the optical absorption window observed experimentally for graphene[19,22,23], this window in a 3DDES is also caused by the different energy requirements for the inter- and intra-band electronic transition channels. v) In a Na_3Bi 3DDES, the high-frequency edge of the optical absorption window is located between $5-10$ μm, which fits the results of experiment[28] very well and different from that in graphene in which the high-frequency edge of the optical absorption window is at 0.1 μm[34]. vi) In the long-wavelength regime ($\lambda > 100$ μm), the intra-band electronic transitions contributes mainly to the optical conductivity where both $\sigma_{xx}(\omega)$ and $\sigma_{zz}(\omega)$ increases sharply with the radiation wavelength. This is similar to the dependence of the optical conductivity on the radiation wavelength in the Durde optical conductivity of free electrons.

In Fig. 5, we show the optical conductivities $\sigma_{xx}(\omega)$ and $\sigma_{zz}(\omega)$ as a function of radiation wavelength λ for fixed carrier densities and electronic relaxation time at different temperatures. We find that in the short-wavelength regime, both $\sigma_{xx}(\omega)$ and $\sigma_{zz}(\omega)$ do not depend on temperature. The peaks of the optical absorption in $\sigma_{xx}(\omega)$ and $\sigma_{zz}(\omega)$ depends weakly on temperature, but the width of the optical absorption window becomes narrow with increasing temperature. This is because E_F^e decreases and E_F^h increases with increasing temperature (see Fig. 2). In such a case, the energy gap $E_F^e - E_F^h$ for inter-band transitions decreases with increasing temperature due to Pauli blockade effect[38,39], so that the photon energy required for inter-band transitions decreases with increasing temperature (see Fig. 3). Furthermore, the decrease in E_F^e and the increases in E_F^h with increasing temperature imply that intra-band electronic transitions need a slightly larger photon energy to overcome the effect of thermal broadening of the electron distribution function. It is interesting to notice that a little kink of $\sigma_{xx}(\omega)$ can be seen at $T = 300$ K at the high frequency edge of the optical absorption window. When $N_e = 2.0\times10^{19}$ cm^{-3}, E_F^e for $T = 0$ K is well above the Berry curvature regime in conduction band (see Fig. 2). With increasing T, E_F^e decreases and E_F^e is located inside the Berry curvature regime. The change of the electron DoS due to the effect of the Berry curvature is the reason for the observation of this kink in $\sigma_{xx}(\omega)$ at $T = 300$ K. Moreover, it can be seen that there is a crossover of both $\sigma_{xx}(\omega)$ and $\sigma_{zz}(\omega)$ at the high frequency edge of the optical absorption window. Similar effect was observed theoretically in graphene-based 2D Dirac systems[34].

In the calculations we take the electronic energy relaxation time τ as an input parameter that takes into account the effect of the broadening of the scattering states. The dependence of $\sigma_{xx}(\omega)$ and $\sigma_{zz}(\omega)$ on τ is shown in Fig. 6 for a fixed temperature and fixed electron and hole densities. A longer energy relaxation time corresponds to a smaller broadening of the scattering state and, thus, to a sample with higher carrier mobility. We note that in the short-wavelength regime, both $\sigma_{xx}(\omega)$ and $\sigma_{zz}(\omega)$ do not depend on the energy relaxation time τ and the corresponding optical absorption peaks do not change with varying τ. Thus, τ mainly affects the intra-band electronic transition. As shown in Fig. 6, both $\sigma_{xx}(\omega)$ and $\sigma_{zz}(\omega)$ in the long-wavelength regime show red shifts with increasing τ. Hence, a wider window in the absorption spectrum can be observed for a larger τ or for a Na_3Bi sample with a larger electron mobility.

In Fig. 7, we show optical conductivities $\sigma_{xx}(\omega)$ and $\sigma_{zz}(\omega)$ as a function of radiation wavelength λ at fixed temperature, electronic relaxation time and hole density for different electron densities N_e. In the short-wavelength regime, both $\sigma_{xx}(\omega)$ and $\sigma_{zz}(\omega)$ do not depend on the electron density. Blue shifts of the optical absorption peak and of the window can be found with increasing electron density. This is because E_F^e increases with N_e so that the inter- and intra-band electronic transitions require larger photon energies for electrons going from lower occupied states to higher empty states by the absorption of the photons. The blue shift of the optical absorption peak can be more obviously observed for $\sigma_{xx}(\omega)$. In Fig. 7, we also show the case with the carrier densities $N_e = 1.0\times10^{18}$ cm^{-3} and $N_h = 1.0\times10^{17}$ cm^{-3}. In this case, E_F^e is inside the conduction band Berry curvature regime. We find that at fixed temperature, the high-frequency edge of the optical absorption window is sharper when E_F^e is above the

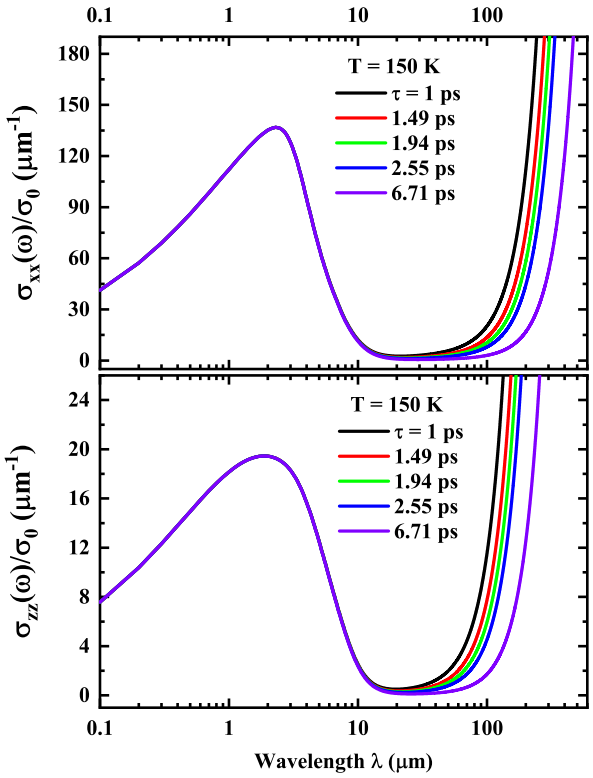

FIG. 6. The dependence of $\sigma_{xx}(\omega)$ (upper panel) and $\sigma_{zz}(\omega)$ (lower panel) on radiation wavelength at a fixed temperature $T = 150$ K and fixed carrier densities $N_e = 2.0 \times 10^{19}$ cm^{-3} and $N_h = 2.0 \times 10^{18}$ cm^{-3} for different electronic relaxation times $\tau = 1$ ps (black curves), 1.49 ps (red curves), 1.94 ps (green curves), 2.55 ps (blue curves), and 6.71 ps (purple curves).

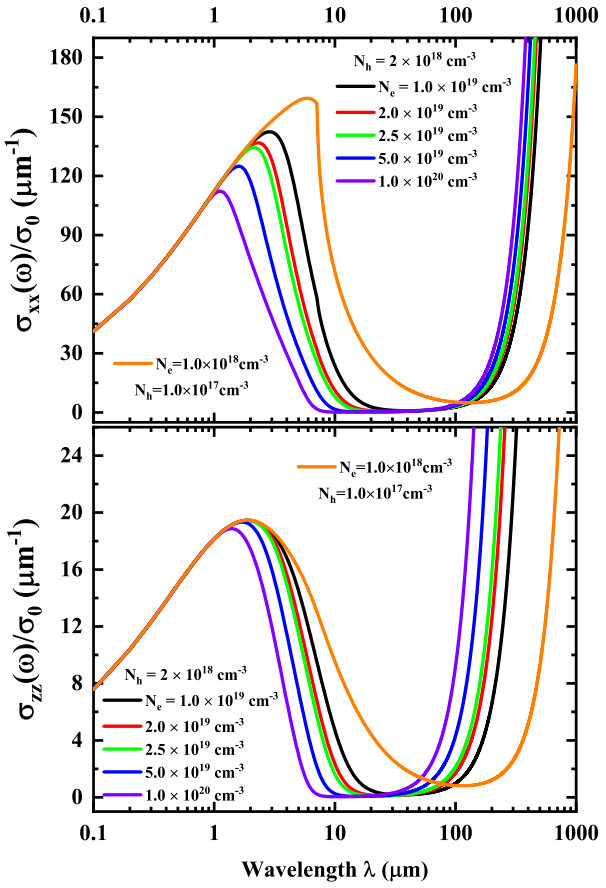

FIG. 7. Optical conductivity spectra σ_{xx} (upper panel) σ_{zz} (lower panel) at fixed temperature $T = 150$ K, electronic relaxation time $\tau = 6.71$ ps, hole density $N_h = 2.0 \times 10^{18}$ cm^{-3} for different electron densities: $N_e = 1.0 \times 10^{19}$ cm^{-3} (black curve), 2.0×10^{19} cm^{-3} (red), 2.5×10^{19} cm^{-3} (green), 5.0×10^{19} cm^{-3} (blue), 1.0×10^{20} cm^{-3} (purple). We also show the corresponding results for a low carrier density sample $N_e = 1.0 \times 10^{18}$ cm^{-3} and $N_h = 1.0 \times 10^{17}$ cm^{-3} (orange curve).

Berry curvature regime than when E_F^e is inside the Berry curvature regime. The degree of sharpness for the low-frequency edge of the optical absorption window depends very weakly on the electron density. This suggests that the presence of the Berry curvature affects mainly the high-frequency edge of the optical absorption window, i.e., the inter-band electronic transitions. From Fig. 7, we notice that the position of the optical absorption peak and window depend sensitively on the electron density. From graphene we know that the inter-band optical absorption channel can be switched on and off when E_F^e is larger or smaller than $\hbar\omega/2$, which is a consequence of the linear like electron energy spectrum in graphene[34]. The results shown in Fig. 7 indicate that akin to graphene-based 2D Dirac electronic systems, the inter-band optical absorption can also be turned on and off by varying the Fermi energy or electron density in Na_3Bi based 3DDESs by, e.g., applying a gate voltage. Thus, this material can also be used as electro-optical modulators. Furthermore, it should be mentioned that graphene based electro-optical modulators work in the mid-infrared regime $\lambda \sim 10\ \mu m$[24,25,34]. Na_3Bi based electro-optical modulator should also work in the mid-infrared bandwidth $\lambda \sim 10\ \mu m$ according to the results obtained from this study.

The results shown in Figs. 4-7 indicate that in the short-wavelength regime where inter-band electronic transitions dominate, the optical conductivities $\sigma_{xx}(\omega)$ and $\sigma_{zz}(\omega)$ for Na_3Bi based 3DDES do not depend on temperature, electron density, and electronic relaxation time, similar to the case of graphene. However in our case, $\sigma_{xx}(\omega)$ and $\sigma_{zz}(\omega)$ depend sensitively on radiation frequency along with the appearance of the optical absorption peak. This is the main difference of the optical conductivity between graphene and Na_3Bi 3DDES. Moreover, because Na_3Bi based 3DDES is a bulk material with different electronic energy spectra along different crystal directions, the optical conductivity $\sigma_{xx}(\omega)$ is always larger than $\sigma_{zz}(\omega)$ regardless of temperature, electron density and relaxation time. This implies that a stronger effect on the optical absorption can be achieved by the radiation field polarized along the 2D plane of Na_3Bi.

IV. CONCLUSIONS

In this study, we have calculated the optical conductivity for Na_3Bi based three-dimensional Dirac electronic system (3DDES) by using a simplified $\mathbf{k}\cdot\mathbf{p}$ model and the energy-balance equation approach based on the semi-classical Boltzmann equation. The effect of light polarization along different crystal directions has been taken into account. For n-type 3DDESs, we have examined the effect of the Berry curvature in the conduction band on the optical conductivity, i.e., optical absorption. Furthermore, we have compared the results with those from a 2DDES such as graphene. The main conclusions drawn from this study are summarized as follows.

For short radiation wavelength radiation ($\lambda <\sim 2\ \mu m$), the optical conductivities $\sigma_{xx}(\omega)$ and $\sigma_{zz}(\omega)$ are induced mainly through inter-band electronic transitions accompanied by the absorption of a photon. In this regime, $\sigma_{xx}(\omega)$ and $\sigma_{zz}(\omega)$ depend on the radiation frequency and an optical absorption peak can be observed. This is the main difference from the high-frequency optical conductivity for a 2DDES such as graphene where $\sigma(\omega)=e^2/4\hbar$ is universal, and this difference is a consequence of the 3D nature of the electronic band structure of Na_3Bi single crystal. However, both $\sigma_{xx}(\omega)$ and $\sigma_{zz}(\omega)$ do not depend on temperature and sample parameters such as electron density and electronic relaxation time, similar to the case of graphene. In the intermediate radiation wavelength regime ($5\mu m<\lambda <\sim 200\mu m$), a strong effect of the absorption window can be observed in both $\sigma_{xx}(\omega)$ and $\sigma_{zz}(\omega)$. Similar to graphene, this window is induced by the different energies that are required for the intra- and inter-band electronic transition channels. Therefore, the width, height, and position of the optical absorption window depend sensitively on temperature, electron density, and electronic relaxation time. We find that the presence of the Berry curvature in the conduction band affects mainly the high-frequency edge of the optical absorption window. In the long radiation wavelength regime ($\lambda >\sim 100\ \mu m$), the intra-band electronic transitions contribute mainly to the optical conductivity, where both $\sigma_{xx}(\omega)$ and $\sigma_{zz}(\omega)$ increase sharply with radiation wavelength. This is similar to the dependence of the optical conductivity on the radiation wavelength of the Durde optical conductivity for free electrons. Moreover, we have found that in a Na_3Bi based 3DDES, $\sigma_{xx}(\omega)$ is about five times larger than $\sigma_{zz}(\omega)$ in short-wavelength regime, regardless of temperature, electron density and relaxation time. This effect is a consequence of the crystal structure of Na_3Bi in which the xy-plane is a layered structure stacked along the z-axis. Thus, a larger optical conductivity or absorption can be achieved by radiation field polarized along the 2D plane of Na_3Bi.

From the viewpoint of device applications, the most significant theoretical finding from this study is that akin to graphene-based 2DDES, the inter-band optical absorption channel can also be turned on and off by varying the Fermi energy or electron density in Na_3Bi based 3DDESs by, e.g., applying a gate voltage. Hence, Na_3Bi based 3DDESs can also be used as electro-optical modulators working in the mid-infrared bandwidth $\lambda\sim 10\ \mu m$. We hope that our interesting theoretical results presented and discussed here can be verified experimentally and can lead to the application of 3DDESs in advanced optoelectronic materials and devices.

ACKNOWLEDGMENTS

This work was supported by the National Natural Science foundation of China (U1930116, U1832153, 11764045, 11574319, 11847054) and the Center of Science and Technology of Hefei Academy of Science (2016FXZY002). Applied Basic Research Foundation of Department of Science and Technology of Yunnan Province (No. 2019FD134), the Department of Education of Yunnan Province (No. 2018JS010), the Young Backbone Teachers Training Program of Yunnan University, and by the Department of Science and Technology of Yunnan Province.

DATA AVAILABILITY

The data that support the findings of this study are available from the corresponding author upon reasonable request.

APPENDIX

Based on the eigenfunction [see Eq. (4)] and the carrier-photon interaction Hamiltonian for the cases where light polarization is along the x- and the z-direction of Na_3Bi [see Eqs. (5) and (6)], by using the Fermi's golden rule

$$W^{j}_{\lambda\lambda'}(\mathbf{K},\mathbf{K}') = \frac{2\pi}{\hbar}|\langle\lambda',\mathbf{K}'|H'_j|\mathbf{K},\lambda\rangle|^2 \times\delta(E_{\lambda'}(\mathbf{K}')-E_{\lambda}(\mathbf{K})-\hbar\omega), \tag{A1}$$

with $j=x$ or z, we can calculate the first-order steady-state electronic transition rate induced by carrier-photon interactions via photon absorption scattering. When $j=x$, we have

$$|\langle\lambda',\mathbf{K}'|H'_x|\mathbf{K},\lambda\rangle|^2 = \left(\frac{eF_0}{\omega\hbar}\right)^2 a_{\mathbf{K}}a^*_{\mathbf{K}}\left|\int e^{-i\mathbf{K}'\cdot\mathbf{R}}e^{i\mathbf{K}\cdot\mathbf{R}}d\mathbf{R}\right|^2 \times\left|\begin{pmatrix}1 & b^*_{\mathbf{K}}\end{pmatrix}\begin{pmatrix}(M_2-C_2)k_x & -A/2\\ -A/2 & -(M_2+C_2)k_x\end{pmatrix}\begin{pmatrix}1\\ b_{\mathbf{K}}\end{pmatrix}\right|^2, \tag{A2}$$

for the x-direction light polarization and When $j=z$, we have

$$|\langle\lambda',\mathbf{K}'|H'_z|\mathbf{K},\lambda\rangle|^2 = \left(\frac{eF_0k_z}{\omega\hbar}\right)^2 a_{\mathbf{K}}a^*_{\mathbf{K}}\left|\int e^{-i\mathbf{K}'\cdot\mathbf{R}}e^{i\mathbf{K}\cdot\mathbf{R}}d\mathbf{R}\right|^2 \times\left|\begin{pmatrix}1 & b^*_{\mathbf{K}}\end{pmatrix}\begin{pmatrix}(M_1-C_1) & 0\\ 0 & -(M_1+C_1)\end{pmatrix}\begin{pmatrix}1\\ b_{\mathbf{K}}\end{pmatrix}\right|^2, \tag{A3}$$

for the z-direction light polarization with $\mathbf{R}=(x,y,z)$, $a_{\mathbf{K}}=Ak(\xi^2_{\lambda\mathbf{K}}+A^2k^2)^{-1/2}$, $b_{\mathbf{K}}=\lambda\xi_{\lambda\mathbf{K}}/Ak_-$, $k=\sqrt{k_x^2+k_y^2}$, $\xi_{\lambda\mathbf{K}}=\sqrt{M_{\mathbf{K}}+A^2k^2}-\lambda M_{\mathbf{K}}$, and $\lambda=+1$ refers to conduction band

and $\lambda = -1$ to valance band. Here, we get $\int e^{-i\mathbf{K}'\cdot\mathbf{R}} e^{i\mathbf{K}\cdot\mathbf{R}} d\mathbf{R} = \delta_{\mathbf{K}',\mathbf{K}}$ and

$$\begin{aligned} |\langle\lambda',\mathbf{K}'|H'_j|\mathbf{K},\lambda\rangle|^2 &= \left(\frac{eF_0}{\omega\hbar}\right)^2 |U^j_{\lambda\lambda'}(\mathbf{K})|^2 \delta_{\mathbf{K}',\mathbf{K}} \\ &= \left(\frac{eF_0}{\omega\hbar}\right)^2 \frac{\delta_{\mathbf{K}',\mathbf{K}} |G^j_{\lambda\lambda'}(\mathbf{K})|^2}{[\xi^2_{\lambda\mathbf{K}} + A^2k^2][\xi^2_{\lambda'\mathbf{K}} + A^2k^2]}, \end{aligned} \tag{A4}$$

with

$$\begin{aligned} G^x_{\lambda\lambda'}(\mathbf{K}) &= A^2(\lambda k_+ \xi_{\lambda\mathbf{K}} + \lambda' k_- \xi_{\lambda'\mathbf{K}})/2 \\ &\quad - k_x[A^2k^2(M_2 - C_2) - \lambda\lambda'(M_2 + C_2)\xi_{\lambda\mathbf{K}}\xi_{\lambda'\mathbf{K}}], \end{aligned}$$

and

$$G^z_{\lambda\lambda'}(\mathbf{K}) = k_z[A^2k^2(M_1 - C_1) - (M_1 + C_1)\lambda\lambda'\xi_{\lambda\mathbf{K}}\xi_{\lambda'\mathbf{K}}].$$

Consequently, the first-order steady-state electronic transition rate induced by carrier-photon interactions via photon absorption scattering is given by Eq. (7).

Once we had the electronic transition rate $W^j_{\lambda\lambda'}(\mathbf{K},\mathbf{K}')$ [see Eq. (7)], we can calculate the optical conductivity of Na_3Bi through the energy-balance equation [Eq. (10)] derived from the semi-classical Boltzmann equation [Eq. (9)]. While we try to get the optical conductivity of Na_3Bi, we choose to take $\mathbf{K} = (k, kz, \phi)$ for calculations. By considering the effect of the broadening of the scattering states due to energy relaxation, i.e., by taking $\delta(E) \to (E_\tau/\pi)(E^2 + E_\tau^2)^{-1}$ (where $E_\tau = \hbar/\tau$) in Eq. (7) with τ being the energy relaxation time, we can calculate the optical conductivity induced by different transition channels from $\sigma_{jj}(\omega) = \sum_{\lambda,\lambda'} \sigma^{\lambda\lambda'}_{jj}(\omega) = \frac{2\hbar\omega}{F_0^2} \sum_{\lambda,\lambda'} \sum_{\mathbf{K},\mathbf{K}'} F^j_{\lambda\lambda'}(\mathbf{K},\mathbf{K}')$. As a result, we have

$$\begin{aligned} \sigma^{\lambda\lambda}_{jj}(\omega) &= \frac{g_s\hbar\omega}{2F_0^2} \frac{1}{(2\pi)^3} \int_0^{2\pi} d\phi \int_{-\infty}^{+\infty} dk_z \int_0^{+\infty} dk k \\ &\quad \times f_\lambda(E_\lambda(\mathbf{K}))[1 - f_\lambda(E_\lambda(\mathbf{K}))] W^j_{\lambda\lambda}(\mathbf{K},\mathbf{K}) \\ &= \frac{g_s\hbar\omega}{2F_0^2} \frac{1}{(2\pi)^2} \left(\frac{eF_0}{\omega\hbar}\right)^2 \frac{2\pi}{\hbar} \delta(-\hbar\omega) \\ &\quad \times \int_{-\infty}^{+\infty} dk_z \int_0^{+\infty} dk k \\ &\quad \times f_\lambda(E_\lambda(\mathbf{K}))[1 - f_\lambda(E_\lambda(\mathbf{K}))] |U^j_{\lambda\lambda}(\mathbf{K})|^2 \end{aligned} \tag{A5}$$

for intra-band transitions and

$$\begin{aligned} \sigma^{-+}_{jj}(\omega) &= \frac{g_s\hbar\omega}{2F_0^2} \frac{1}{(2\pi)^3} \int_0^{2\pi} d\phi \int_{-\infty}^{+\infty} dk_z \int_0^{+\infty} dk k \\ &\quad \times f_-(E_-(\mathbf{K}))[1 - f_+(E_+(\mathbf{K}))] W^j_{-+}(\mathbf{K},\mathbf{K}) \\ &= \frac{g_s\hbar\omega}{2F_0^2} \frac{1}{(2\pi)^2} \left(\frac{eF_0}{\omega\hbar}\right)^2 \frac{2\pi}{\hbar} \int_{-\infty}^{+\infty} dk_z \int_0^{+\infty} dk k \\ &\quad \times f_-(E_-(\mathbf{K}))[1 - f_+(E_+(\mathbf{K}))] |U^j_{-+}(\mathbf{K})|^2 \\ &\quad \times \delta(E_-(\mathbf{K}) - E_+(\mathbf{K}) - \hbar\omega) \end{aligned} \tag{A6}$$

for inter-band transitions.

With Eqs. (A5), (A6) and (8), by taking $j = x$ or z, we obtained the optical conductivity of Na_3Bi induced by different transition channels in different light polarizations as Eqs. (12-15).

[1] K. S. Novoselov, A. K. Geim, S. V. Morozov, D. Jiang, Y. Zhang, S. V. Dubonos, I. V. Grigorieva, and A. A. Firsov, Science **306**, 666 (2004).
[2] M. J. Allen, V. C. Tung, and R. B. Kaner, Chem. Rev. **110**, 132 (2009).
[3] S. M. Young, S. Zaheer, J. C. Y. Teo, C. L. Kane, E. J. Mele, and A. M. Rappe, Phys. Rev. Lett. **108**, 140405 (2012).
[4] M. Neupane, S. Y. Xu, R. Sankar, N. Alidoust, G. Bian, C. Liu, I. Belopolski, T. R. Chang, H. T. Jeng, H. Lin, A. Bansil, F. C. Chou, and M. Z. Hasan, Nat. Commun. **5**, 3786 (2014).
[5] Z. K. Liu, B. Zhou, Y. Zhang, Z. J. Wang, H. M. Weng, D. Prabhakaran, S.-K.Mo, Z. X. Shen, Z. Fang, X. Dai, Z. Hussain, and Y. L. Chen, Science **343**, 864 (2014).
[6] J. L. Mañes, Phys. Rev. B **85**, 155118 (2012).
[7] Sihang Liang, Jingjing Lin, Satya Kushwaha, Jie Xing, Ni Ni, R. J. Cava, and N. P. Ong, Phys. Rev. X **8**, 031002 (2018).
[8] P. E. C. Ashby and J. P. Carbotte, Phys. Rev. B **89**, 245121 (2014).
[9] S. Y. Xu, C. Liu, S. K. Kushwaha, R. Sankar, J. W. Krizan, I. Belopolski, M. Neupane, G. Bian, N. Alidoust, T. R. Chang, H. T. Jeng, C. Y. Huang,W. F. Tsai, H. Lin, P. P. Shibayev, F. C. Chou, R. J. Cava, and M. Z. Hasan, Science **347**, 294 (2015).
[10] S. Ebihara, K. Fukushima, and T. Oka, Phys. Rev. B **93**, 155107 (2016).
[11] C. M. Wang, Hai-Zhou Lu, and Shun-Qing Shen, Phys. Rev. Lett. **117**, 077201 (2016).
[12] C. Zhang, Y. Zhang, X. Yuan, S. H. Lu, J. L. Zhang, A. Narayan, Y. W. Liu, H. Q. Zhang, Z. L. Ni, R. Liu, E. S. Choi, A. Suslov, S. Sanvito, L. Pi, H.-Z. Lu, A. C. Potter, and F. X. Xiu, Nature (London) **565**, 331 (2019).
[13] Zehua Huang, Yadong Jiang, Qi Han, Ming Yang, Jiayue Han, Fang Wang, Man Luo, Qing Li, He Zhu, Xianchao Liu, Jun Gou, and Jun Wang, Nanotechnology (2019).
[14] Ming Yang, Jun Wang, Yunkun Yang, Qi Zhang, Chunhui Ji, Guorong Wu, Yuanjie Su, Jun Gou ,Zhiming Wu, Kaijun Yuan, Faxian Xiu, and Yadong Jiang, J. Phys. Chem. Lett. 2019, **10**, 14, 3914-3921.
[15] Wei Lu, Jiwei Ling, Faxian Xiu, and Dong Sun, Phys. Rev. B **98**, 104310 (2018).
[16] K. S. Novoselov, A. K. Geim, S. V. Morozov, D. Jiang, M. I. Katsnelson, I. V. Grigorieva, S. V. Dubonos, and A. A. Firsov, Nature (London) **438**, 197 (2005).
[17] Y. Q. Wu, K. A. Jenkins, A. Valdes-Garcia, D. B. Farmer, Y. Zhu, A. A. Bol, C. Dimitrakopoulos, W. J. Zhu, F. N. Xia, P. Avouris, and Y.-M. Lin, Nano Lett. **12**, 3062 (2012).
[18] Q. L. Bao, H. Zhang, B. Wang, Z. H. Ni, C. H. Y. X. Lim, Y. Wang, D. Y. Tang, and K. P. Loh, Nat. Photonics **5**, 411 (2011).
[19] A. B. Kuzmenko, E. van Heumen, F. Carbone, and D. van der Marel, Phys. Rev. Lett. **100**, 117401 (2008).
[20] F. Wang, Y. Zhang, C. Tian, C. Giri, A. Zettl, M. Crommie, and Y. Ron Shen, Science **320**, 206 (2008).
[21] J. M. Dawlaty, S. Shivaraman, J. Strait, P. George, M. Chandrashekhar, F. Rana, M. G. Spencer, D. Veksler, and Y. Q. Chen, Appl. Phys. Lett. **93**, 131905 (2008).
[22] L. A. Falkovsky and S. S. Pershoguba, Phys. Rev. B **76**, 153410 (2007).
[23] V. Ryzhii, M. Ryzhii, and T. Otsuji, J. Appl. Phys. **101**, 083114 (2007).
[24] H. J. Haugan, F. Szmulowicz, G. J. Brown, and K. Mahalingam, J. Appl. Phys. **96**, 2580 (2004).
[25] H. Mohseni and M. Razeghi, IEEE Photonics Technol. Lett. **13**, 517 (2001).
[26] Satya K. Kushwaha, Jason W. Krizan, Benjamin E. Feldman, Andrs Gyenis, Mallika T. Randeria, Jun Xiong, Su-Yang Xu, Nasser Alidoust, Ilya Belopolski, Tian Liang, M. Zahid Hasan, N. P. Ong, A. Yazdani, and R. J. Cava, APL Materials **3**, 041504 (2015).
[27] Z. J. Wang, Y. Sun, X. Q. Chen, C. Franchini, G. Xu, H. M. Weng, X. Dai, and Z. Fang, Phys. Rev. B **85**, 195320 (2012).
[28] G. S. Jenkins, C. Lane, B. Barbiellini, A. B. Sushkov, R. L. Carey, Fengguang Liu, J. W. Krizan, S. K. Kushwaha, Q. Gibson, Tay-Rong Chang, Horng-Tay Jeng, Hsin Lin, R. J. Cava, A. Bansil, and H. D. Drew, Phys. Rev. B **94**, 085121 (2016).
[29] N. P. Armitage, E. J. Mele, and Ashvin Vishwanath Rev. Mod. Phys. **90**, 015001 (2018).

[30] H. F. Yuan, W. Xu, X. N. Zhao, D. Song, G. R. Zhang, Y. M. Xiao, L. Ding, and F. M. Peeters, Phys. Rev. B **99**, 235303 (2019).
[31] Z. Wang, H. Weng, Q. Wu, X. Dai, and Z. Fang, Phys. Rev. B **88**, 125427 (2013).
[32] J. Xiong, S. K. Kushwaha, T. Liang, J. W. Krizan, M. Hirschberger, W. D. Wang, R. J. Cava, and N. P. Ong, Science **350**, 413 (2015).
[33] J. Xiong, S. Kushwaha, J. Krizan, T. Liang, R. J. Cava, and N. P. Ong, Europhys. Lett. 114, 27002 (2016).
[34] H. M. Dong, J. Zhang, F. M. Peeters, and W. Xu, J. Appl. Phys. **106**, 043103 (2009); W. Xu, H. M. Dong, L. L. Li, J. Q. Yao, P. Vasilopoulos, and F. M. Peeters, Phys. Rev. **B 82**, 125304 (2010).
[35] W. Xu, F. M. Peeters, and J. T. Devreese, Phys. Rev. B **43**, 14134 (1991).
[36] W. Xu, Phys. Rev. B **71**, 245304 (2005).
[37] E. N. Economou, Greens functions in quantum physics (Third editon) (Berlin, Springer-Verlag, 2006).
[38] E. Burstein, Phys. Rev. **93**, 632 (1954).
[39] H. J. Krenner, E. C. Clark, T. Nakaoka, M. Bichler, C. Scheurer, G. Abstreiter, and JJ. Finley, Phys. Rev. Lett. **97**, 076403 (2006).